ON THE MOTION OF AN OSCILLATING BUBBLE IN AN ELASTIC LIQUID

Daniel Lima Albernaz, daniellima2006@gmail.com
Francisco Ricardo Cunha, frcunha@unb.br
University of Brasilia, Department of Mechanical Engineering, Brasilia-DF, Brazil

Abstract. *In this paper we investigate the motion of a single oscillating bubble in a viscoelastic fluid. The constitutive equation for the fluid has been based on a Maxwell model with an extensional viscosity for the viscous contribution. This viscoelastic model results in a second order nonlinear integro-differential governing equation that might be integrated by using a fifth order Runge-Kutta scheme with adaptive time step. The numerical computation solves three first order ordinary differential equations, including the one associated with the solution of the convolution integral. In addition, it is also presented an asymptotic solution of the bubble dynamics for small values of the elastic parameter (i.e. Deborah number). While the extensional viscosity is related to the strong anisotropy produced in the flow by the stretched macromolecule, the elastic part of the model represents the relaxation time of the additive. Results of the nonlinear response of the bubble as a function of the elastic and the anisotropic parameters are presented.*

Keywords: *bubble, convolution integral, viscoelastic, extensional viscosity*

1. INTRODUCTION

The development of the study of bubble dynamics started with problems presented by the first ship propellers initially constructed, due to their inefficiency caused by the presence of water vapor bubbles on the blades. Despite the unwanted effects cavitation provides in performance or vibrations for many mechanical processes, the non-linear dynamics of bubbles discovered applications in numerous areas. For instance, cavitation plays an important role in protein folding (Brinker et al., 2006), as well as in breaking up harmful molecules found in water (Dahi, 1982). The subject also has concerns to recent biomedical fields (Allen and Roy, 2000). The stress field generated by cavitation induces comminution of kidney stones (Lokhandwalla and Sturtevant, 2000). Moreover, an innovative proposal consists on the use of ultrasound-induced cavitation for safe and efficient drug delivery, for chemotherapy treatment (Liu, Miyoshi and Nakamura, 2006). However, cavitation can become a source of unwanted collateral effects, limiting the place for its application (Sehgal and Wang, 1981). The dynamical response of a spherical oscillating bubble largely appears in literature, nevertheless its behavior when immersed in a non-newtonian fluid still requires much progress. Related works from Ting, 1978 and Chahine and Fruman, 1979 showed that bubble oscillations in non-linear fluids composed by polymer solution are attenuated compared to a Newtonian fluid. The relation between the factors responsible for the bubble collapse attenuation phenomenon is uncertain; the role of the extensional viscosity due to the particle extensions versus the elastic effects in this physical mechanism is still an ongoing subject of debate.

We propose a study of a single oscillating bubble immersed in a viscoelastic fluid, undergoing an acoustic pressure field. The ambient fluid is characterized as a substance composed of a Newtonian liquid and a dilute volume fraction of additives as long fibers or few ppm of macromolecules. The constitutive equation for the fluid has been based on a Maxwell model, combining an extensional viscosity (for the viscous contribution) and elastic effects. While the extensional viscosity is related to the strong anisotropy produced in the flow by the stretched macromolecule, the elastic contribution of the model represents the relaxation of the additives.

An extension of the classical Rayleigh-Plesset equation is developed, where we take into account the boundary conditions in the bubble interface. The equation is solved numerically, integrated by using a fifth order Runge-Kutta scheme with appropriated time steps. The referred model involves a convolution or memory integral, resulting into a non-linear integro-differential equation which governs the bubble dynamics. The solution of the integro-differential equation is obtained by the Newton-Leibniz transformation of the original second order ordinary differential equation into a system with three non-linear first order equations, including an ordinary differential equation for the convolution integral. This procedure is used in the context of different flows involving non-Newtonian fluid with memory (Jiménez-Fernández and Crespo, 2006). An asymptotic solution is proposed, by an integration by parts. The convergence of the resulting series is validated by a comparison with the numerical integration by the Runge-Kutta scheme aforementioned. With an appropriated dimensionless analysis of the governing equation it is possible to identify the following physical parameters: Reynolds number, Re, the Weber number, We and the Deborah number, De. The influence of these on the bubble motion are investigated.

2. MATHEMATICAL FORMULATION

The bubble is considered immersed in a Newtonian incompressible fluid of viscosity μ and density ρ, containing a volume fraction of anisotropic particles of length ℓ and diameter a. The inner side of the bubble is composed by a mixture of contaminant gas (which develops a polytropic process) and liquid vapor. This mixture acts like a energy cushion of the liquid while the bubble contracts. We assume that the bubble maintains a spherical shape and develops only radial motions due to superficial tension, simplifying our analysis to an unidimensional motion. Factors that could be able to change the sphericity of the bubble, like pressure gradients in the liquid, presence of gravitational field or surfactants are neglected.

No mass flux in the liquid-gas interface is considered because this phenomenon only has relevant dynamical effects at very low ambient pressure and for great portion of vapor in the mixture inside the bubble. The pressure inside the bubble is supposed to be spatially uniform and non-equilibrium effects in the collapse instant are not taken into account. Furthermore, heat conduction through the bubble wall is negligible. The general governing equations for the motion of an incompressible fluid are given by the continuity equation

$$\nabla \cdot \mathbf{u} = 0\,, \tag{1}$$

and the momentum equation

$$\rho\left(\frac{\partial \mathbf{u}}{\partial t} + \mathbf{u}\cdot\nabla\mathbf{u}\right) = \nabla\cdot\mathbf{\Sigma}\,, \tag{2}$$

where $\mathbf{u}$ is the Eulerian velocity field and $\mathbf{\Sigma}$ is the stress tensor of the flow. Now, considering a radial flow i.e., $\mathbf{u} = u_r$, in a spherical coordinate system with origin at the center of the bubble, Eqs. (1) and (2) lead to the well-known Rayleigh-Plesset equation for describing bubble dynamics. Hence:

$$\ddot{R}R + \frac{3}{2}\dot{R}^2 = \frac{p_\ell(R,t) - p_\infty(t)}{\rho}\,. \tag{3}$$

Here R represents the bubble radius as a function of time. The dot indicates time differentiation. The term $p_\infty(t)$ is the transient ambient pressure that excites the system and $p_\ell(R,t)$ denotes the liquid pressure, defined by the boundary conditions in the bubble interface.

2.1 Constitutive Model

The Maxwell model consists of a combination between a damp (viscous contribution) and a spring (elastic effects), in series connection. The Maxwell model is described by the following superposition of deformation rates:

$$\dot{\gamma} = \dot{\gamma}_e + \dot{\gamma}_v\,, \tag{4}$$

with $\dot{\gamma}$ being the total rate of deformation, $\dot{\gamma}_v$ presents the rate of viscous deformation and $\dot{\gamma}_e$ is the rate of elastic deformation. We consider $\sigma = \dot{\gamma}_v\mu_e$, where μ_e denotes the extensional viscosity and σ denotes the stress applied by the flow. Also we have $\dot{\sigma} = \dot{\gamma}_e G$, where G corresponds to the elastic modulus. Equation (4) becomes:

$$\dot{\sigma} + \frac{1}{\alpha}\sigma = \frac{\mu_e}{\alpha}\dot{\gamma}\,, \tag{5}$$

where $\alpha = \mu_e/G$ represents the relaxation time of the elastic fluid. For the problem examined here the rate of deformation is defined as $\dot{\gamma} = \mathbf{D} : \mathbf{ss}$, where $\mathbf{s}$ is the unit vector in the additive orientation direction and $\mathbf{D}$ is the rate of strain tensor, given by $\mathbf{D} = 1/2(\nabla u + (\nabla u)^T)$. Note that if $\alpha = 0$, we recover a pure anisotropic model with extensional viscosity (i.e. without elastic effects). Using the integrating factor method, after few algebraic manipulations we achieve:

$$\sigma(R,t) = -2\frac{\mu_e}{\alpha}\int_{-\infty}^{t} e^{\frac{-(t-\tau)}{\alpha}}\frac{\dot{R}(\tau)}{R(\tau)}d\tau\,, \tag{6}$$

with τ being the time variable of the integration, and t the current time of the motion. Equation (6) represents an integro-differential equation, or convolution integral. The bulk stress tensor for a statistically homogeneous suspension is given by Cunha, 1995, as

$$\mathbf{\Sigma} = -p\mathbf{I} + 2\mu\mathbf{D} + 2\mathbf{\Sigma}^f\,, \tag{7}$$

where p represents the pressure field, $\mathbf{I}$ is the identity tensor and $\mathbf{\Sigma}^f$ denotes the extra stress tensor due to additive particles, which assumes the form:

$$\mathbf{\Sigma}^f = 2\sigma(R,t)\mathbf{ss} \Rightarrow \mathbf{\Sigma} = -p\mathbf{I} + 2\mu\mathbf{D} + 2\sigma(R,t)\mathbf{ss}\,. \tag{8}$$

At the bubble interface we consider continuity of tangential stresses and velocity. On the other hand a discontinuity in the normal stresses occurs due to surface tension. In this case the jump of the normal stress is given by:

$$[\![\Sigma_{nn}]\!] = (\mathbf{n}\cdot\boldsymbol{\Sigma}\cdot\mathbf{n})_\ell - (\mathbf{n}\cdot\boldsymbol{\Sigma}\cdot\mathbf{n})_b = \Gamma 2\bar{\kappa}\,. \tag{9}$$

Here $\mathbf{n}$ is the flow direction (unit normal vector). The term Γ denotes the surface tension coefficient, which is $\bar{\kappa} = 1/R$, for a spherical bubble. The term $(\mathbf{n}\cdot\boldsymbol{\Sigma}\cdot\mathbf{n})_b$ represents the normal component of the traction for the bubble inner side, while $(\mathbf{n}\cdot\boldsymbol{\Sigma}\cdot\mathbf{n})_\ell$ is related to the normal component of the traction on the suspension side. Analyzing each contribution on the right hand side of equation (9) we have, respectively:

$$(\mathbf{n}\cdot\boldsymbol{\Sigma}\cdot\mathbf{n})_b = -p_b(t) \tag{10}$$

$$(\mathbf{n}\cdot\boldsymbol{\Sigma}\cdot\mathbf{n})_\ell = -\mathbf{n}\cdot p_\ell(R,t)\mathbf{I}\cdot\mathbf{n} + \mathbf{n}\cdot\left[2\mu\mathbf{D} + 2\boldsymbol{\Sigma}^f\right]\cdot\mathbf{n}\,. \tag{11}$$

Here $p_b(t)$ is the bubble internal pressure, evaluated by $p_b(t) = p_v + p_g(t)$, where p_v refers to the liquid vapor pressure inside the bubble and $p_g(t)$ is the contaminant gas pressure (which is assumed to describe a polytropic process, i.e., $p_g V^n = constant$). The term $\mathbf{n}\cdot\mathbf{D}\cdot\mathbf{n}$ is expressed by:

$$\mathbf{n}\cdot\mathbf{D}\cdot\mathbf{n} = \left.\frac{\partial u}{\partial r}\right|_{r=R} = -2\frac{\dot{R}}{R}\,. \tag{12}$$

Using the expression of $\mathbf{n}\cdot\boldsymbol{\Sigma}^f\cdot\mathbf{n} = \sigma(R,t)$ defined in Eq. (6) and $\mathbf{n}\cdot\mathbf{D}\cdot\mathbf{n}$ given by Eq. (12), Eq. (11) reduces to:

$$(\mathbf{n}\cdot\boldsymbol{\Sigma}\cdot\mathbf{n})_\ell = -p_\ell(R,t) - 4\mu\frac{\dot{R}}{R} - 4\frac{\mu_e}{\alpha}\int_{-\infty}^{t} e^{\frac{-(t-\tau)}{\alpha}}\frac{\dot{R}(\tau)}{R(\tau)}d\tau\,. \tag{13}$$

Now, substituting Eqs. (10) and (13) into Eq. (9), one obtains:

$$p_\ell(R,t) = p_v + \left((\tilde{p}_\infty - p_v) + \frac{2\sigma}{R_E}\right)\left(\frac{R_E}{R}\right)^{3n} - \frac{2\sigma}{R} - 4\mu\frac{\dot{R}}{R} - 4\frac{\mu_e}{\alpha}\int_{-\infty}^{t} e^{\frac{-(t-\tau)}{\alpha}}\frac{\dot{R}(\tau)}{R(\tau)}d\tau\,, \tag{14}$$

where $\tilde{p}_\infty$ represents the statical pressure for an equilibrium condition and R_E is the bubble equilibrium radius. The forcing acoustic pressure field is defined by $p_\infty(t) = \tilde{p}_\infty(1 + \varepsilon\sin(\omega t))$, where ε represents the pressure amplitude and ω is the forcing pressure frequency. Now with p_ℓ expressed by Eq. (14), a modified Rayleigh-Plesset equation may be written as:

$$\begin{aligned}\ddot{R}R + \frac{3}{2}\dot{R}^2 &= -\frac{\Delta\tilde{p}}{\rho} + \frac{1}{\rho}\left(\Delta\tilde{p} + \frac{2\sigma}{R_E}\right)\left(\frac{R_E}{R}\right)^{3n} - \frac{2\sigma}{R\rho} - \frac{\tilde{p}_\infty}{\rho}\varepsilon\sin(\omega t)\\ &- \frac{4\mu}{\rho}\frac{\dot{R}}{R} - 4\frac{\mu_e}{\rho\alpha}\int_{-\infty}^{t} e^{\frac{-(t-\tau)}{\alpha}}\frac{\dot{R}(\tau)}{R(\tau)}d\tau\,,\end{aligned} \tag{15}$$

where $\Delta\tilde{p} = \tilde{p}_\infty - p_v$.

2.2 Non-dimensional formulation

First we define dimensionless variables, which are indicated by asterisks as follows:

$$R^* = \frac{R}{R_E}\,, \qquad t^* = \frac{t}{t_c}\,, \tag{16}$$

where $U_c = \left(|\Delta\tilde{p}|/\rho\right)^{1/2}$ and $t_c = R_E/U_c$ represent typical scales of velocity and time, respectively. Thus, the non-dimensional form of Eq. (15) results in:

$$\begin{aligned}R^*\ddot{R}^* + \frac{3}{2}(\dot{R}^*)^2 &= \frac{2}{\mathrm{We}}\left(\frac{1}{(R^*)^{3n}} - \frac{1}{R^*}\right) - 1 - \varepsilon^*\sin(\omega t) + \frac{1}{(R^*)^{3n}} - \frac{4}{\mathrm{Re}}\frac{\dot{R}^*}{R^*}\\ &- \frac{4}{\mathrm{Re}}\frac{1}{De}f^*\int_{-\infty}^{t^*} e^{-\frac{(t^*-\tau^*)}{De}}\frac{\dot{R}^*(\tau^*)}{R^*(\tau^*)}d\tau^*\,.\end{aligned} \tag{17}$$

Here f^* is a material function, which corresponds to the ratio μ_e/μ. The following physical parameters were identified:

$$\mathrm{Re} = \frac{\rho U_c R_E}{\mu} \ , \ \mathrm{We} = \frac{\rho U_c^2 R_E}{\sigma} \ , \ De = \frac{\alpha}{t_c} \ , \tag{18}$$

where Re corresponds to the Reynolds number (i.e. the relation between inertia and viscous forces) and We is the Weber number, which denotes the ratio of inertia and surface tension forces. In particular, the Deborah number De is the relevant elastic parameter, which represents the ratio of the relaxation time and characteristic timescale for the bubble wall motion. It should be important to note that the excitation amplitude ε was redefined in Eq. (18) as $\varepsilon^* = \varepsilon\,(\Delta\tilde{p}/\tilde{p}_\infty)$. Batchelor, 1970, has developed a model for the extensional viscosity, based on a slender body theory for a dilute rigid-rod suspension. He found that:

$$f^* = \frac{\mu_e}{\mu} = \frac{4\pi}{3}\frac{(n_d \ell^3)}{ln(\ell/a)} = \frac{4}{3}\left(\frac{\ell}{a}\right)^2 \frac{\phi}{ln(\ell/a)} \ , \tag{19}$$

where n_d represents the number of additives per unit volume and ℓ/a is the additive aspect ratio. The theory is considered for elongated additives at low Reynolds number, with additives fully oriented in the radial direction. Equation (19) is satisfied for a dilute regime (i. e., $n_d \ell \ll 1$). For cylindrical particles, $n_d \ell^3 = (\phi/\pi)(\ell/a)^2$, where ϕ denotes the additive volume fraction. A second order model for f^* was proposed by Shaqfeh and Frederickson, 1990. These authors have expanded Batchelor's theory for a semi-diluted suspension ($\phi \ll 1 \ll n_d \ell^3$), finding that:

$$f^* = \frac{4}{3}\left(\frac{\ell}{a}\right)^2 \frac{\phi}{ln(1/\phi)}\left[1 - \frac{ln(ln(1/\phi))}{ln(1/\phi)} + \frac{E(\phi)}{ln(1/\phi)}\right] \ . \tag{20}$$

Equation (20) takes into account the effect of two-particle hydrodynamic interaction, where $E(\phi)$ depends on the particle volume fraction (e.g. for aligned cylindrical particles, $E(\phi) = 0.1585$). Equation (20) is used in the present work.

2.3 Numerical solution

In order to simplify the problem, we write the convolution memory integral as follows:

$$I(R^*, t^*) = \int_{-\infty}^{t^*} e^{-\frac{(t^*-\tau^*)}{De}} \frac{\dot{R}^*(\tau^*)}{R^*(\tau^*)} d\tau^* \ . \tag{21}$$

Now, using the Newton-Leibniz formula, Eq. (21) is derived with respect to time, giving:

$$\begin{aligned} \frac{d}{dt^*}\left(I(R^*, t^*)\right) &= \frac{\dot{R}^*(t^*)}{R^*(t^*)} - \frac{1}{De}\int_{-\infty}^{t^*} e^{-\frac{(t^*-\tau^*)}{De}} \frac{\dot{R}^*(\tau^*)}{R^*(\tau^*)} d\tau^* \\ \dot{I}(R^*, t^*) &= \frac{\dot{R}^*(t^*)}{R^*(t^*)} - \frac{1}{De} I(R^*, t^*) \ . \end{aligned} \tag{22}$$

Equation (22) is needed to solve the full governing equation described in Eq. (17), as being a system of three first order differential equations. The resulting initial value problem is integrated using a fifth order Runge-Kutta scheme with an adaptive time step (Press et al., 1992). The algorithm is based on the Fehlberg method (Cash and Karp, 1990). The input datas of the simulations are De, Re, We, ϕ, R_0 (initial radius), ℓ/a, ω, I_0 (initial value of the convolution integral), ε, $\dot{R}_0$ (initial velocity) and the parameters that control interactions and the adaptive time steps. A difficult problem in bubble dynamics simulations is the control of time steps and the prediction of the collapse. Computation time tends to be higher in the neighborhood of the collapse point, which may be avoided. We have developed a theory in order to predict the bubble collapse radius, and use it to extrapolate the numerical solution at times close to the collapse event.

3. PRELIMINARY ANALYSIS

3.1 An asymptotic solution for the governing equation

An asymptotic solution for the convolution integral in Eq. (6) is obtained by means of successive integrations by parts. The solution is found in terms of a power series written in terms of Deborah number is given by

$$A(R^*, t^*) = \sum_{k=1}^{N} (-1)^k 2\mu_e De^{(k-1)} \frac{d^{(k-1)}}{dt^{*(k-1)}}\left(\frac{\dot{R}^*(t^*)}{R^*(t^*)}\right) \ . \tag{23}$$

For the first three terms, the serine in Eq. (23) reduces to

$$A(R^*,t^*) = -2\mu_e\frac{\dot{R}^*}{R^*} + 2\mu_e De\left[\frac{\ddot{R}^*}{R^*} - \left(\frac{\dot{R}^*}{R^*}\right)^2\right] - 2\mu_e De^2\left[\frac{R^{(3)*}}{R^*} - 3\frac{\ddot{R}^*\dot{R}^*}{(R^*)^2} + 2\left(\frac{\dot{R}^*}{R^*}\right)^3\right] + O(De^3). \quad (24)$$

Figure 1 shows the variation of the convolution integral $I(t)$ as a function of De, for both contribution of the asymptotic solution ($O(De)$ (dotted line) and $O(De^2)$) (dashed line with points) and also the numerical solution (solid line). A comparison between analytical and numerical integration points out that as the Deborah number increases the series converges only for the $O(De)$ contribution. When $De \to 0$, the asymptotic solutions $O(De)$, $O(De^2)$ and the numerical solution are in very good agreement. However, it is seen that for $De > 0.1$, the series expansion $O(De^2)$ presents a different convergence from the numerical solution. So, the analytical solution converge at first order, $O(De)$. Therefore

$$A(R^*,t^*) = -2\mu_e\frac{\dot{R}^*}{R^*} + 2\mu_e De\left[\frac{\ddot{R}^*}{R^*} - \left(\frac{\dot{R}^*}{R^*}\right)^2\right] , \quad (25)$$

for $De \to 0$.

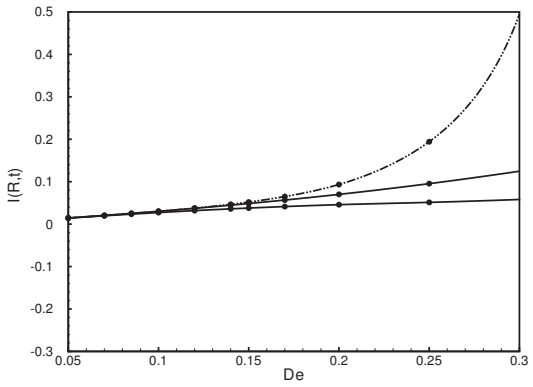

Figure 1. Integral $I(R,t)$ as a function of the Deborah number. Solid line: numerical solution; dotted line: $O(De)$; dashed line with points: $O(De^2)$.

3.2 An asymptotic theory for the bubble collapse

An efficient way of dealing with bubble dynamics is first to establish a minimum radius R_{col}, which consists of the value when collapse occurs. This critic radius is considered as the lowest value between an asymptotic minimum radius developed (R_{min}) and the van der Waals radius R_{vw}, denoted as the maximum packing factor achieved by the contaminant gas molecules within the bubble. Represented by van der Waals hard core, it has been assumed in the present work that $R_{vw} \sim 1/10R_0$ (Löfstedt et al., 1995, suggested $R_{vw}/R_0 \sim 1/8$, for air).

Now, we propose an asymptotic theory in order to predict the bubble collapse radius. Consider the most severe condition of the flow (i.e. $\mathrm{Re} \to \infty$), where the viscous term is neglected ($\mu \to 0$). With a constant ambient pressure, $p_\infty(t) = \tilde{p}_\infty$, Eq. (15) reduces to

$$\ddot{R}R + \frac{3}{2}\dot{R}^2 = -\frac{\Delta\tilde{p}}{\rho} + \frac{1}{\rho}\left(\Delta\tilde{p} + \frac{2\sigma}{R_E}\right)\left(\frac{R_E}{R}\right)^{3n} - \frac{2\sigma}{R\rho} . \quad (26)$$

So, making use of the integrating factor, for an isothermal process ($n = 1$), we have:

$$\frac{d}{dt}\left(R^3\dot{R}^2\right) = -\frac{2}{3}\left(\frac{\Delta\tilde{p}}{\rho}\right)\frac{d}{dt}\left(R^3\right) + \frac{2}{\rho}\tilde{G}\frac{d}{dt}(\ln R) - \frac{2\sigma}{\rho}\frac{d}{dt}\left(R^2\right) , \quad (27)$$

where $\tilde{G} = (\Delta\tilde{p} + 2\sigma/R_E)R_E^3$ is an equilibrium constant. For the initial conditions $R(0) = R_0$ and $\dot{R}(0) = 0$, and integrating Eq. (27), results in:

$$\dot{R}^2 = \left(\frac{R_0^3}{R^3}\right)\left[\frac{2}{3}\left(\frac{\Delta\tilde{p}}{\rho}\right)\left(1 - \frac{R^3}{R_0^3}\right) + \frac{2}{\rho}\tilde{G}\frac{1}{R_0^3}ln\left(\frac{R}{R_0}\right) - \frac{2\sigma}{\rho}\frac{1}{R_0}\left(\frac{R^2}{R_0^2} - 1\right)\right] . \quad (28)$$

Nearby to the collapse, the bubble radius goes to zero (i.e. $R \ll R_0$). Under this condition, Eq. (28) reduces to:

$$\dot{R}^2 = \left(\frac{R_0^3}{R^3}\right)\left[\frac{2}{3}\frac{\Delta\tilde{p}}{\rho} + \frac{2}{\rho}\tilde{G}\frac{1}{R_0^3}ln\left(\frac{R}{R_0}\right) + \frac{2\sigma}{\rho}\frac{1}{R_0}\right] . \tag{29}$$

Considering that if the bubble radius reaches a minimum, $\dot{R} = 0$ must be satisfied, Eq. (29) may be solved to give

$$\ln\left(\frac{R}{R_0}\right) = -\frac{R_0^3}{3\tilde{G}}\left(\Delta\tilde{p} + \frac{3\sigma}{R_0}\right) . \tag{30}$$

Therefore, as $R = R_{min}$ leads to

$$R_{min} = R_0 e^{-\left[\frac{R_0^3}{3\tilde{G}}\left(\Delta\tilde{p}+\frac{3\sigma}{R_0}\right)\right]} . \tag{31}$$

In terms of dimensionless quantities Eq. (31) assumes the form

$$R^*_{min} = R^*_0 e^{-(R^*_0)^2\left[\frac{1+R^*_0 \mathrm{We}/3}{\mathrm{We}+2}\right]} . \tag{32}$$

As before, the radius are non-dimensionalized by R_E. Note that the criterion for collapse is dependent of the bubble initial radius, for a finite Weber number (Fogler and Goddard, 1970). In order to save computation time, we develop a semi-theoretical equation for describing the bubble radius evolution at configurations close to the collapse condition, given by Eq. (32). Theoretical refinement is used in order to improve the control of the bubble minimum collapse radius. Therefore, when defining R_{min} as a function of R_0, it results in different curves for a given We. This plot is presented in Figure 2, where both asymptotic limits (We $\to 0$ and We $\to \infty$) are showed as well.

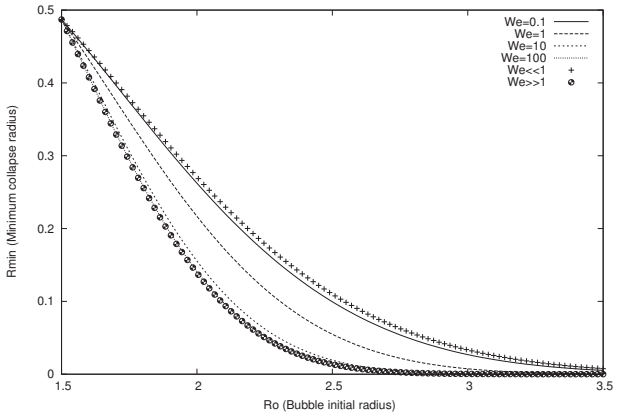

Figure 2. Minimum bubble radius R_{min} as a function of the initial radius R_0 for several Weber numbers (i.e. We $=$ 0.1; 1; 10; 100). The asymptotical limits We $\to 0$ ($R_{min} = R_0 e^{-R_0^2/2}$) and We $\to \infty$ ($R_{min} = R_0 e^{-R_0^3}$) are also showed.

It should be important to note that the saturation $R_0 \to 0$ is out of the limit application of the proposed theory, since it requires that $R \ll R_0$. Hence, it is considered values of $R \sim 1$. Figure 2 indicates that for high We (i.e. low surface tension effect compared to inertia), as the bubble contracts, the surface tension is not sufficient to equilibrate the strong external pressure, resulting on a lower value presented for R_{min}.

The opposite physical situation occurs at the asymptotical limit We $\to 0$, when the surface tension in very small bubble radius strongly reacts to the external pressure, increasing R_{min} significantly. As a complementary result, R_{min} as a function of We is presented in Figure 3, for different values of R_0. It is seen that R_{min} decreases accordingly to the increasing of the We parameter. In particular, Figure 3 shows that We ~ 5 should be considered as the saturation condition corresponding to high We. When We $= 5$, $R_{min} \cong 0$ for $R_0 = 3.0$ and $R_{min} \cong 0.02$ for $R_0 = 2.5$.

4. RESULTS AND DISCUSSIONS

In this work bubble dynamics has been examined by integrating Eq. (17) with the following initial conditions: $R_0 = 1$, $\dot{R}_0 = 0$ and $I_0 = 0$. The focus is to investigate the nonlinear response of a single bubble immersed in a viscoelastic fluid. In all numerical simulations, the polytropic coefficient is assumed $n = 1$ and the frequency $\omega = 1$. The Reynolds number also demands limited values, whereas under $\mathrm{Re} > 10^2$, the effect of the liquid rheology on the spherical bubble dynamics may be negligible (Brujan, 1999). However, viscoelastic effects have an increasing quantitative influence as the Reynolds

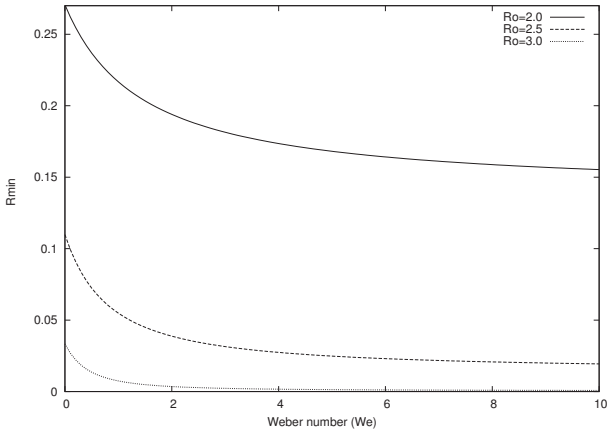

Figure 3. Minimum bubble radius R_{min} as a function of the We parameter, for different R_0 values.

number is reduced. Fig. 4 shows the bubble radius response in a viscoelastic fluid as a function of time, for a particle volume fraction $\phi = 0.3\%$, an aspect ratio $\ell/a = 100$, Re $= 15$, We $= 15$ and a pressure amplitude $\varepsilon = 1$. Fig. 4 (a) shows multiple periods of oscillations whereas Fig. 4 (b) shows a plot of a single period of the bubble oscillatory motion. In these figures, the solid line represents $De = 0$. The dotted line denotes $De = 0.2$ and dashed line with points denotes $De = 0.6$. As $De \to 0$ we have the asymptotic limit with elasticity effects being only a small effect. Actually, this limit corresponds to the anisotropic regime represented by an extensional viscosity, and the additives are fully stretched. The results indicate that as the Deborah number increases, the effect of additive relaxation (i.e. elasticity) produces a bubble oscillatory motion more unstable, representing bifurcations threshold.

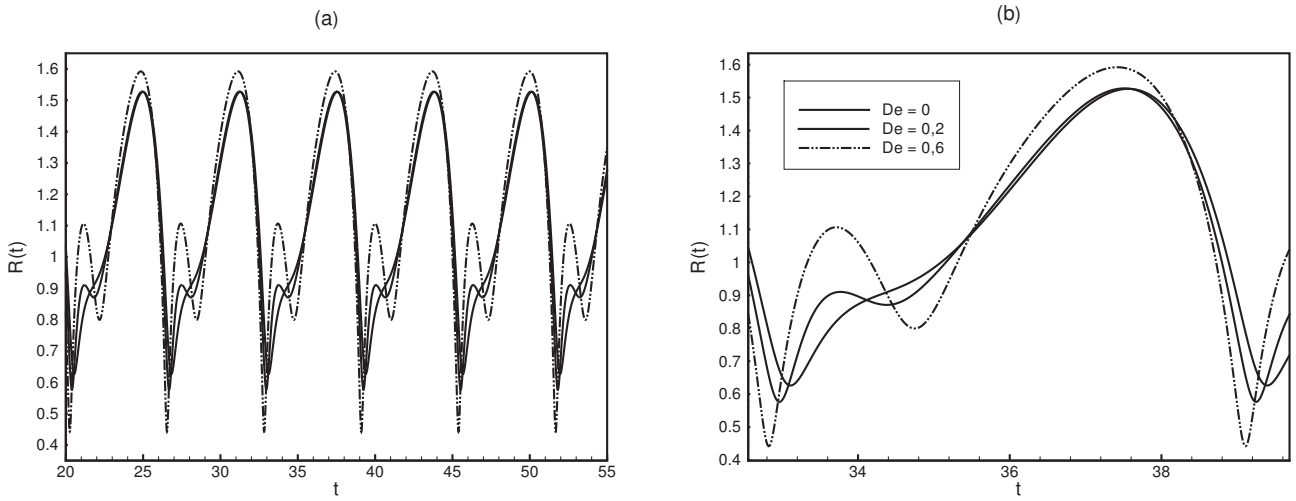

Figure 4. Bubble radius as a function of time, for $\phi = 0.3\%$, $\ell/a = 100$, Re $= 15$, We $= 15$ and $\varepsilon = 1$. (a) a plot with multiple periods and (b)a plot of a single period. Solid line: $De = 0$ (i.e. the elasticity effects are neglected); dotted line: $De = 0.2$; dashed line with points: $De = 0.6$.

Figure 5 shows the behavior of the bubble internal pressure and the bubble surface velocity, respectively. The plot (a) presents the variations of the internal pressure of the bubble , p_b, as a function of time and, (b) denotes the bubble surface velocity $\dot{R}$ as a function of time. Again, solid lines represent $De = 0$, dotted lines $De = 0.2$ and dashed lines with points $De = 0.6$. Fig. 5 (a) shows higher picks of the pressure amplitude inside the bubble as the influence of elasticity on the bubble motion increases. It is seen that the sharp points take place when the bubble contracts, reaching $p_b \sim 13$. We can see that during the bubble compression motion the relaxation of the additives (or macromolecules) in the ambient liquid leads to bubble radius smaller than the case in which the elasticity is absent ($De = 0$). Consequently, it is observed higher pressure inside the bubble as De increases. The velocity also presents higher values as De increases. It should be important to note that this coupling between the motion of the bubble and the relaxation of the additive is significant only when the bubble period oscillation is of the same order of magnitude of the additive relaxation time. That means $De \sim 1/\omega$.

The convolution integral I is plotted in Fig. 6. In these plots (a) gives I as a function of time and (b) presents the phase diagram of I (which corresponds to the I rate as a function of I). In particular, fig. 6 shows that the instability

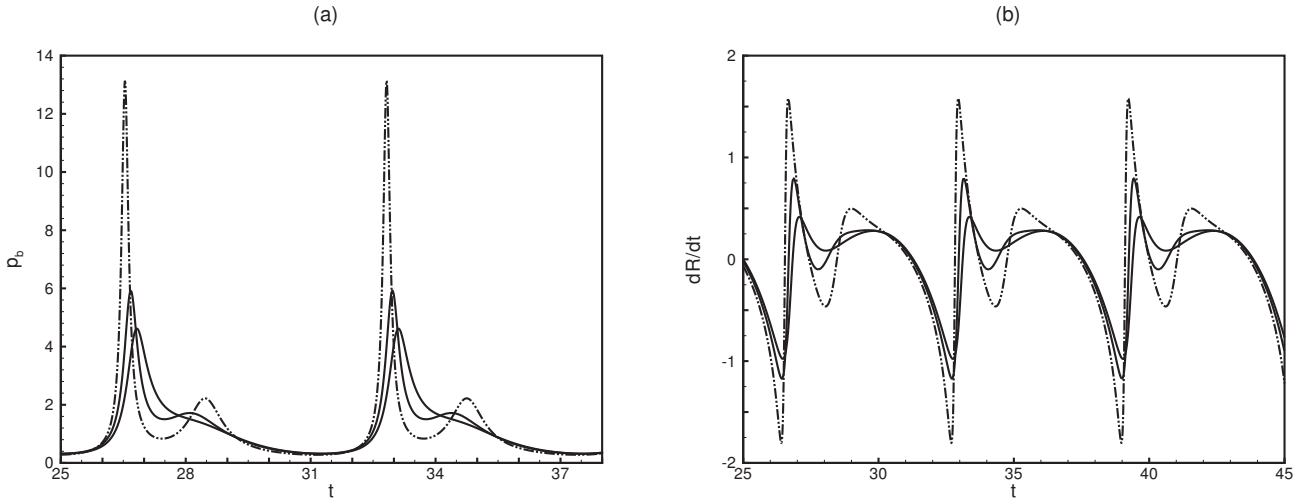

Figure 5. Nonlinear bubble oscillations, for $\phi = 0.3\%$, $\ell/a = 100$, $\mathrm{Re} = 15$, $\mathrm{We} = 15$ and $\varepsilon = 1$. (a) internal bubble pressure as function of time; (b) bubble surface velocity as function of time. Solid line: $De = 0$; dotted line: $De = 0.2$; dashed line with points: $De = 0.6$.

of the oscillatory behavior is enhanced by the elasticity of the fluid, accelerating the route to the bubble collapse. These findings predicted by the proposed viscoelastic are in qualitative agreement with several works available in the literature (e.g. Tanasawa and Yang, 1970, Shima et al., 1988 and Kim, 1994).

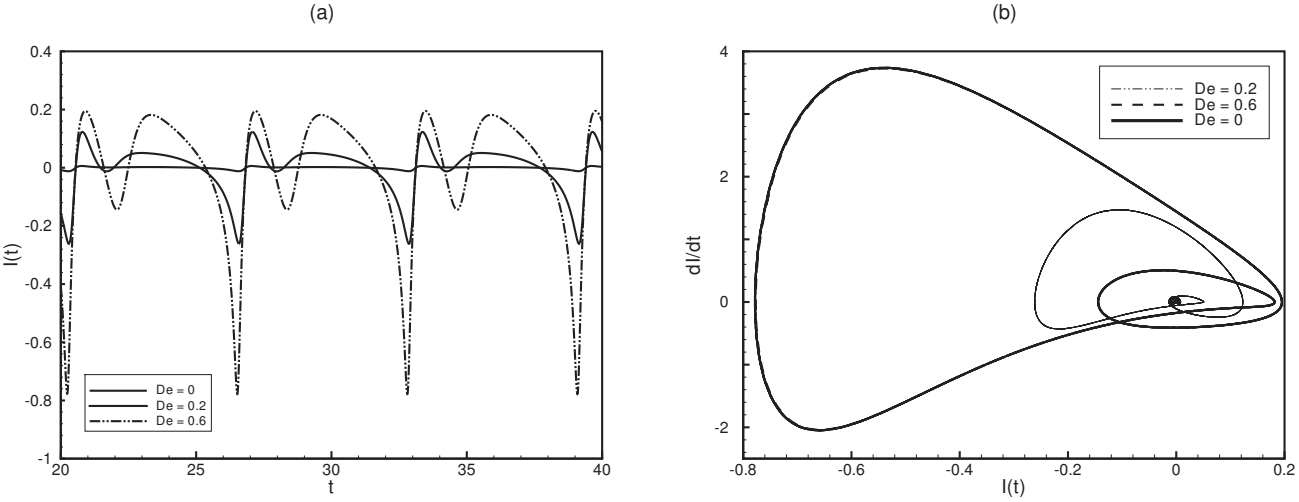

Figure 6. Dynamical behavior of I for different De numbers. (a) I integral as a function of time; (b) dI/dt as a function of I (phase diagram). Solid line: $De = 0$; dotted line: $De = 0.2$; dashed line with points: $De = 0.6$.

Figure 7 shows the bubble radius evolution, for $De = 0$ (solid line), $De = 1$ (dotted line) and $De = 5$ (dashed line with points). The plots certify a significant influence of the additive elasticity (measured by the De numbers) in the bubble response. It is seen only a small difference between the plots corresponding to $De = 1$ and $De = 5$. This result could be expected since for $De \sim 1$ the additives tend to become fully stretched such as rigid fibres. In particular a $De = 5$ means that the relaxations time of the additive is five times bigger than the typical period of the forcing bubble oscillation ($\omega = 1$). Under these conditions the motion of the bubble is not changed by the effect of additive relaxation (i.e. its elasticity).

Figure 8 shows a plot of the maximum radius of the bubble R_{max} as a function of the Deborah number De, for different particle volume fractions. The solid line denotes $\phi = 0.1\%$, the dotted line $\phi = 0.3\%$ and the dashed line with points $\phi = 0.5\%$. The elastic regime corresponds to region of $De \sim 1$, where the relaxation time is of the order of the flow time. This regime is bounded by the two asymptotic limits mentioned above (i.e. $De \to 0$, and $De \gg 1$). In both limits, our model consider that the additives are fully stretched, and they behave like rigid fibres. This anisotropy is characterized in terms of an extensional viscosity of the ambient liquid around the bubble. The results of Figure 8 indicates that, as the additive volume fraction is enhanced, the effect of the additive elastic relaxation on the bubble is increased giving the

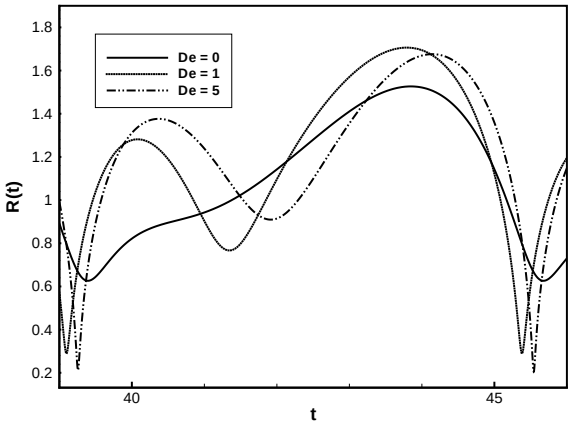

Figure 7. Bubble radius as a function of time; Here $\phi = 0.3\%$, $\ell/a = 100$, $\mathrm{Re} = 15$, $\mathrm{We} = 15$ and $\varepsilon = 1$. Solid line: $De = 0$; dotted line: $De = 1$; dashed line with points: $De = 5$.

higher values of R_{max} observed. On the other hand, it is seen that an increasing in the volume fraction of the additive requires stronger flows (i.e. higher De) to stretch the additives. Consequently, it leads to a delay in De for the oscillatory motion of the bubble reaching its maximum radius. It also produces a delay in the anisotropic regime of fully stretched particles. Figure 8 shows that R_{max} for $\phi = 0.5\%$ corresponds to a Deborah number approximately twice the Deborah number associated with R_{max} at $\phi = 0.3\%$.

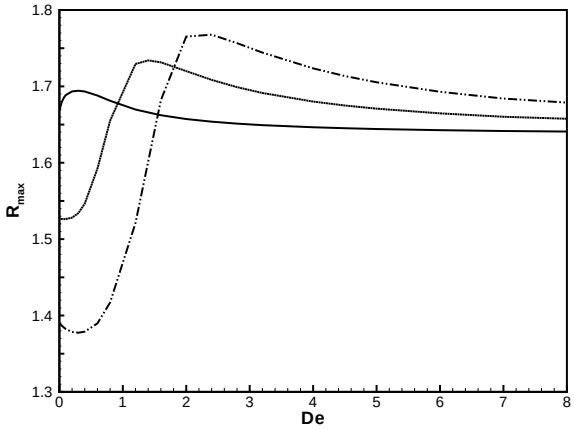

Figure 8. Variation of the maximum radius R_{max} with Deborah number De. Aspect ratio $\ell/a = 100$, $\mathrm{Re} = 15$, $\mathrm{We} = 15$ and $\varepsilon = 1$. Solid line: $\phi = 0.1\%$, dotted line: $\phi = 0.3\%$ and dashed line with points: $\phi = 0.5\%$.

5. CONCLUDING REMARKS

The dynamic behavior of a single bubble immersed in a viscoelastic liquid characterized by a Maxwell model was successfully observed. The integro-differential equation was solved and an analytical solution was proposed. A rigorous study on the eminence of the bubble collapse has been done, including the development of an asymptotical theory for the bubble minimum radius. This theory has been used to extrapolate the results of the numerical simulation for the collapse condition.

The results have shown that the liquid elasticity increases the degree of instability in the oscillatory motion of the bubble. This of course can decrease the collapse time of a cavitating bubble. In particular, when the bubble surface is expanding the additives are experiencing a stretching. In counterpart, during the compressional motion of the bubble the elastic energy stored by the additive contributes during its relaxation time with the contraction of the bubble leading to very small radius. This coupling between the additive elasticity and the bubble oscillatory motions seems to be important only under condition that $De \sim 1/\omega$.

6. ACKNOWLEDGEMENTS

The authors wish to acknowledge the support of this work by CNPq-Brazil and CAPES-Brazil.

7. REFERENCES

Allen, J.S. and Roy, R.A., 2000, "Dynamics of gas bubbles in viscoelastic fluids. I. Linear viscoelasticity", J. Acoust. Soc. Am., Vol. 107, p. 3167–3178.

Batchelor, G.K., 1970, "Slender-body theory for particle of arbitrary cross section in Stokes flow", Journal of Fluid Mechanics, Vol. 44, pp. 419.

Brinker, C.J., Singh, S., Houston, J. and Swol, F.V., 2006, "Drying transition of confined water", Nature, Vol. 442, p. 526.

Brujan, E.A., 1999, "A first-order model for bubble dynamics in a compressible viscoelastic fluid", J. non-Newtonian Fluid Mech., Vol. 84, p. 83–103.

Cash, J.R. and Karp, A.H., 1990, "ACM Transactions on Mathematical Software",Vol. 16, p. 201–222.

Chahine, G.L. and Fruman, D.H., 1979, "Dilute polymer solution effects on bubble growth and collapse", Phys. Fluids, Vol. 22, p. 1406–1407.

Cunha, F.R., 1995, "Hydrodynamics dispersion in suspension", Department of Applied Mathematics and Theoretical Physics, University of Cambridge.

Dahi, E., 1982, Perspective of combination of ozone and ultrasound, Ozonization Manual for Water and Wastewater Treatment, John Wiley and Sons.

Fogler, H.S. and Goddard, J.D., 1970, "Collapse of St'herical Cavities in Viscoelastic Fluids", The Physics Fluids, Vol. 13, p. 1135–1141.

Jiménez-Fernández, J. and Crespo, A., 2006, "The collapse of gas bubbles and cavities in a viscoelastic fluid", International J. of Multiphase Flow, Vol. 32, p. 1294–1299.

Kim, C., 1994, "Collapse of spherical bubbles in Maxwell fluids", J. non-Newtonian Fluid Mech., Vol. 55, p. 37–58.

Liu, Y., Miyoshi, H. and Nakamura, M., 2006, "Encapsulated ultrasound microbubbles: Therapeutic application in drug/gene delivery", Journal of Controlled Release, Vol. 114, p. 89–99.

Lokhandwalla, M. and Sturtevant, B., 2000, "Fracture mechanics model of stone comminution in ESWL and implications for tissue damage", Phys. Med. Biol., Vol. 45, p. 1923–1940.

Löfstedt, R., Weninger, K., Putterman, S. and Barber, B.P., 1995, "Sonoluminescing bubbles and mass diffusion", Physical Review E, Vol. 51, p. 4400–4410.

Press, W.H., Flannery, B.P., Teukolsky, S.A. and Vetterling, W.T., 1992, "Numerical Recipes in Fortran 77", Cambridge University Press.

Sehgal, C.M. and Yang, S.Y., 1981, "Threshold intensities and kinetics of sonoreaction of thymine in aqueous solutions at low ultrasonic intensities, J. Am. Chem. Soc., Vol. 103, p. 6606.

Shaqfeh, E.S.G. and Frederikson, G.H., 1990, "The hydrodynamics stress in a suspension of rods", Phys. Fluids, Vol. 2, p. 7–24.

Shima, A., Tsujino, T. and Oikawa, Y., 1988, "The collapse of bubbles in viscoelastic fluids", Inst. High Speed Mech. Tohoku University, Vol. 55, p. 17–34.

Tanasawa, I. and Yang, W.J., 1970, "Dynamic behavior of a gas bubble in viscoelsatic liquids", J. Appl. Phys., Vol. 41, p. 4526–4531.

Ting, R.Y., 1978, "Characteristics of flow cavitation in dilute solution of polyethilene oxide and polyacrylamide", Phys. Fluids Vol. 21, p. 898–901.